ELSEVIER

Contents lists available at ScienceDirect

International Journal of Heat and Mass Transfer

journal homepage: www.elsevier.com/locate/hmt



Development of differential thermal resistance method for thermal conductivity measurement down to microscale



Mahya Rahbar^{a,1}, Meng Han^{b,1}, Shen Xu^c, Hamidreza Zobeiri^{a,*}, Xinwei Wang^{a,*}

- ^a Department of Mechanical Engineering, Iowa State University, Ames, Iowa 50011, United States of America
- b Shenzhen Institute of Advanced Electronic Materials, Shenzhen Institute of Advanced Technology, Chinese Academy of Sciences, Shenzhen 518055, PR China
- ^c School of Mechanical and Automotive Engineering, Shanghai University of Engineering Science, 333 Longteng Road, Shanghai 201620, PR China

ARTICLE INFO

Article history: Received 25 August 2022 Revised 28 October 2022 Accepted 22 November 2022

Keywords:
Differential thermal resistance (DTR)
Out-of-plane thermal conductivity
In-plane thermal conductivity
Mm/micron scale
Lorenz number

ABSTRACT

The thermal conductivity (k) of materials plays a critical role in the effectiveness of devices in the engineering fields. In this work, a novel differential thermal resistance (DTR) method is developed to measure the out-of-plane and in-plane k of mm- down to μ m-thick samples. Traditional techniques for direct k measurement usually needs measuring the heat transfer and temperature difference across the sample. The DTR technique rather constructs configurations for reference samples and sample of interest to measure the temperature rise and determine the thermal resistance of the sample and its k. Non-contact heating by laser and thermal probing by a high-sensitivity infrared camera are employed. The out-of-plane k of 1.49 and 2.81 mm-thick acrylic samples, and 1 mm-thick glass slide is measured to be 0.20, 0.19, and 1.27 W·m⁻¹·K⁻¹, respectively. The in-plane k of a 26 μ m-thick graphene paper is measured to be 616 W·m⁻¹·K⁻¹. A good level of agreement is obtained between our measurement results and reference values. Moreover, the in-plane k of 15 μ m-thick pure copper foil is measured to be 322 W·m⁻¹·K⁻¹, very well agreeing with the density-adjusted value of 326 W·m⁻¹·K⁻¹ for pure copper. Also by measuring the copper coil's electrical conductivity, we are able to determine its Lorenz number as (2.21-2.30) × 10⁻⁸ W· Ω ·K⁻² which agrees well with reference values of (2.23-2.33) × 10⁻⁸ W· Ω ·K⁻².

© 2022 Elsevier Ltd. All rights reserved.

1. Introduction

Thermal management is a significant challenge in different engineering fields such as electronic packaging [1,2], phase change energy storage [3], and heat sinks [4,5]. Thermal conductivity measurement of materials has received considerable attention due to its important role in the reliability and performance design of devices. To date, many techniques have been developed to measure the thermal conductivity of micro/nanoscale materials, such as flash [6–8], transient electrothermal (TET) [9–11], transient photoelectrothermal (TPET) [12,13], 3ω [14–16], optical heating and electrical thermal sensing (OHETS) [17–19], pulsed laser-assisted thermal relaxation (PLTR) [20–23], time-domain thermo-reflectance (TDTR) [23–25], and frequency-domain thermo-reflectance (FDTR) [26–28] techniques.

In the flash method, first introduced by Parker et al. [6], the front surface of a few mm-thick sample is uniformly irradiated by a short and high-intensity light flash, and the transient tempera-

E-mail addresses: hzobeiri@iastate.edu (H. Zobeiri), xwang3@iastate.edu (X. Wang).

ture rise of the rear surface of the sample is recorded. The thermal diffusivity of the sample is calculated using the time needed for the sample's rear surface to reach half of the maximum temperature, called half-rise time [7,8]. In the TET technique, a suspended sample between two electrodes is fed by a DC step current, and the sample's temperature will increase. Depending on sample length and diffusivity, it takes a millisecond to hundreds of seconds to reach a steady-state. This temperature change is monitored by measuring the transient voltage response of the sample as a function of time. The thermal diffusivity of the sample is obtained by fitting the voltage change against time. This technique is suitable for measuring the thermal properties of metallic, nonconductive, and semi-conductive microscale/nanoscale 1D samples [9–11]. The TPET technique has the same principle as TET, but it uses an amplitude-modulated continuous-wave (CW) laser beam to heat the sample and a small DC current to measure the induced voltage change. Using a small DC current helps reduce heating and improves the measurement accuracy. For short wires with a high thermal conductivity/diffusivity, it is difficult to use TET and TPET since such samples transfer heat to reach a steady-state in a very short period of time, and it is comparable to the rising time of the current source and modulated laser [12,13]. In the 3ω technique, a sine/cosine AC current with an angular frequency of ω and am-

^{*} Corresponding authors.

¹ Equal contribution authors.

plitude of I_0 passes through the sample and causes temperature fluctuation at 2ω frequency. As a result, voltage fluctuation occurs at the 3ω frequency, which is then used for measuring thermal properties. However, this technique has a lower signal-to-noise ratio than TET or TPET, and it is time-consuming and requires minutes to hours to sweep the needed frequencies. It is only applicable to conductive samples and the sample is required to have a linear I-V relationship [14-16]. In the OHETS technique the sample is suspended between two electrodes and irradiated by a periodically modulated laser beam. As a result, a periodical temperature change occurs, and a small DC current is passed through the sample to measure the periodical voltage change. This technique is suitable for conductive, non-conductive, and semi-conductive micro/nanoscale wires [17–19]. However, like the 3ω technique, it has a low signal level and is relatively time-consuming [9].

The PLTR technique is developed to overcome the drawbacks of TET, TPET, 3ω , and OHETS techniques since it is fast and has a high signal-to-noise ratio. In the PLTR technique, a nanosecond or picosecond laser pulse irradiates a suspended sample between two electrodes. As a result, the temperature of the sample increases. After pulsed heating, the sample's temperature will decrease gradually. The temperature relaxation is used to determine the thermal diffusivity of the sample. This technique is suitable for conductive, non-conductive, and semi-conductive wires, as well as short wires with high thermal conductivity [20-22]. Another technique for measuring the thermal conductivity of submicron thin films ranging from 0.03 to 2000 W·m⁻¹·K⁻¹ is the TDTR technique which uses a high-frequency pulsed laser to heat the sample. After the pulsed laser heating, the sample cools down. This temperature variation is measured by a probe pulse and leads to the temperature-dependent properties measurement. This technique has a short thermal diffusion length and a high signal-to-noise ratio. However, the short thermal diffusion length, comparable to the laser spot size, makes TDTR to be more sensitive to the cross-plane direction heat conduction. However, improvements have been done to measure in-plane thermal conductivity $(>10 \text{ W}\cdot\text{m}^{-1}\cdot\text{K}^{-1})$ with this technique [23–25]. The FDTR technique is developed to overcome the TDTR complexity. In this technique, thermo-reflectance signals are monitored as a function of modulation frequency instead of time delay. It helps eliminate the moving delay stage. In addition, both in-plane and cross-plane thermal conductivities can be measured with a single measurement [26-28].

The out-of-plane thermal conductivity of micro-thick samples can be obtained using the laser flash technique. However, samples' density and specific heat are required. In addition, the half-rise time for these samples is in the order of 10^{-5} s or shorter, which makes the measurement more challenging. Moreover, although very high in-plane thermal conductivity of micro-thick samples can be obtained using the TET technique, the samples' high electrical conductivity makes the required electrical hearting hard to apply. To overcome these challenges, in this work, a differential thermal resistance (DTR) method is developed to measure the out-of-plane thermal conductivity of mm- to μ m-thick samples and in-plane thermal conductivity of micro-thick samples while no additional information such as density and specific heat, nor Joule heating is required. In addition, the other advantage of the DTR technique is that its sample preparation is much easier than other techniques we discussed in the paper. However, the disadvantage of the DTR technique is that it is hard to apply to nanoscale samples. To verify this new methodology, thermal conductivity measurement of acrylic glass, glass, graphene paper, and copper foil have been conducted. Our results show good agreement with literature values, which firmly validate the accuracy of the DTR technique.

2. DTR measurement of out-of-plane thermal conductivity

2.1. Measurement principle

The idea of the DTR technique is to construct different thermal circuit scenarios with some having known thermal resistors involved. As a result, the thermal resistance of the sample can be solved precisely and its thermal conductivity can be determined with high confidence. This will eliminate problems of measuring temperature difference and energy flow across the sample while still measuring its thermal conductivity with sound accuracy. In this part, we introduce the DTR method for the out-of-plane thermal conductivity measurement. Figure 1(a) shows the physical principles behind this measurement. The sample is attached to an Aluminum (Al) substrate using a double-side black tape, and its top is also coated with a black tape. A laser (1550 nm wavelength) (Model number: BWF2-1550-2-400-0.22-SMA) is used to irradiate the top tape surface, and the surface temperature rise is measured using an infrared camera (Model number: PI450). In this configuration, the measured temperature rise is determined by the absorbed laser power, the thermal resistance of the sample (R_s) , the thermal resistance of the two black tapes (R_t) , thermal resistance of radiation-convection (R_{rc}) on the top of the sample, and the thermal resistance of the substrate (R_{sub}). The relevant circuit is shown in Fig. 1(b). The laser spot is large enough to cover the entire sample, and the irradiated laser energy is measured using a power meter with sound accuracy. The top black tape will ensure the laser energy is well absorbed with negligible reflection.

In this thermal design, we have several unknown thermal resistances, like those of the black tape, the Al substrate, and convection and radiation. Another configuration (termed "black tape case") is designed as shown in Fig. 1(b), where exactly, and only the same black tapes are used for laser irradiation and temperature rise sensing. The configuration allows us to precisely determine the total thermal resistance of convection, radiation, black tapes and substrate. This information is still not sufficient for us to determine the thermal resistance of the sample $R_{\rm S}$. Therefore, a third configuration (reference case) is designed, which is very similar to the sample measurement case, but using a glass sample of known thermal conductivity to replace the sample. Figure 1(c) shows the uniform temperature distribution of this experiment's black tape, sample, and glass. It is obvious the sample's surface has a very uniform temperature, with a nonuniformity better than 0.3 °C.

High-purity fused glass (fused silica) with a given thermal conductivity (k_g =1.4 W·m⁻¹·K⁻¹ [29]) and known thickness (t_g =1.578 mm) is used in the reference case. Its thermal resistance is $R_g = t_g/(k_gA_g) = 1.578 \times 10^{-3}/(1.4 \times 64 \times 10^{-6}) = 1772 \text{ K} \cdot \text{W}^{-1}$. Here, A_g is the glass surface area. Note in our experiment all three configurations are controlled to have the same cross-sectional area of 8 × 8 mm². Details of uncertainty analysis are provided later. The thermal conductivity of the sample is obtained using this equation $k_s = t_s/(R_sA_s)$. Here, t_s is the sample thickness which is measured by a digital micrometer, and A_s is cross-sectional area of the sample which is 64 mm². For all the three thermal circuits in Fig. 1(b), the governing equations are:

$$Q_{tot} = \Delta T_{tot} \left[\frac{1}{R_{rc}} + \frac{1}{R_{tot}} \right], \tag{1}$$

$$Q_{\rm s} = \Delta T_{\rm s} \left[\frac{1}{R_{\rm rc}} + \frac{1}{R_{\rm tot} + R_{\rm s}} \right],\tag{2}$$

$$Q_g = \Delta T_g \left[\frac{1}{R_{rc}} + \frac{1}{R_{tot} + R_g} \right]. \tag{3}$$

Here, the subscript "tot" represents combinations of two tapes and the Al substrate. Q_{tot} , Q_s , Q_g , ΔT_{tot} , ΔT_s , and ΔT_g are the absorbed

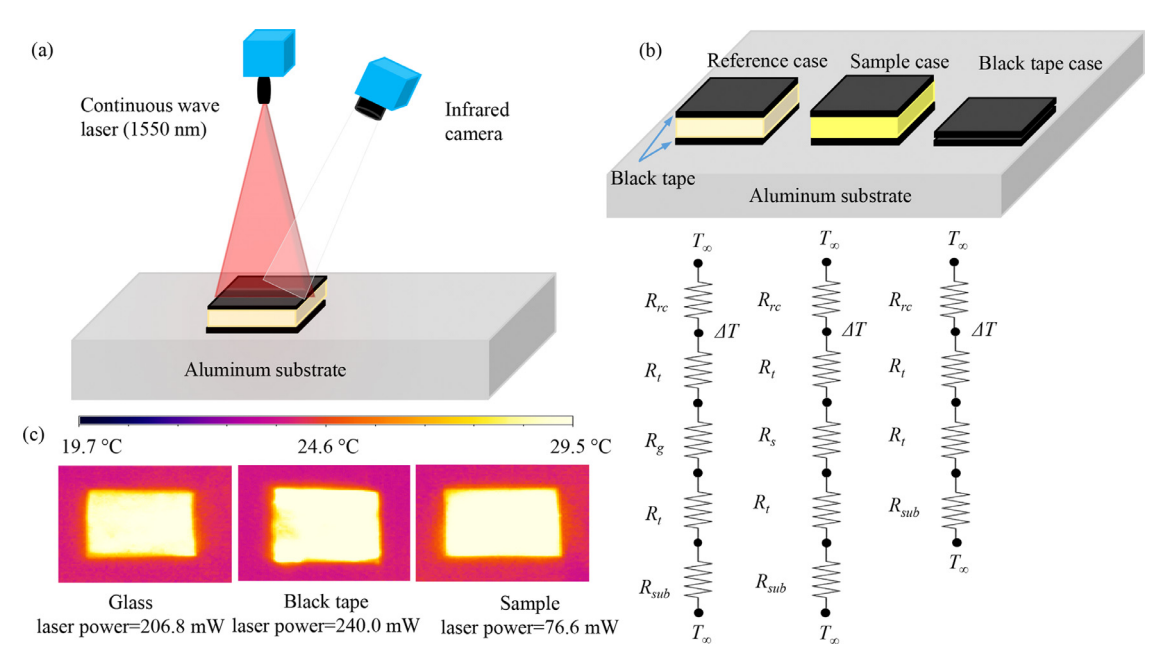


Figure 1. (a) Physical principles of DTR for out-of-plane thermal conductivity measurement, (b) different configurations and corresponding thermal resistance circuits of the DTR method. The thermal resistance symbols are: R_{rc} for radiation and convection, R_t for black tape, R_g for glass, R_{sub} for Al substrate, and R_s for the sample, and (c) temperature distribution of three typical measurements. (Not to scale.)

Table 1 Experimental details of 1 mm-thick glass sample.

	Sample size			T_1 [°C]	<i>T</i> ₂ [°C]	Δ <i>T</i> [°C]	Q [mW]
Sample	Length [mm]	Width [mm]	Thickness [mm]				
Tape (2 layers)	8	8	0.66	23.0	27.7	4.70	248
Glass (pure fused silica)	8	8	1.59	22.8	30.7	7.90	248
Glass slide	8	8	1.00	23.0	30.0	7.00	248

laser powers and temperature rise for the tape, sample, and glass (reference) cases, respectively. Solving this equation group will determine the thermal resistance of the sample R_s .

2.2. Measurement of reference materials

In this part, the thermal conductivity of one-millimeter-thick normal microscope glass slide (plain microscope slides from Fisher) and two acrylic samples (extruded acrylic from TAP Plastics) is measured using the DTR method to access its measurement accuracy. Table 1 shows the details of the glass slide's experiment. In this table, T_1 and T_2 represent the temperature of configurations before and after laser irradiation. ΔT is the temperature rise caused by laser irradiation. The glass slide's thermal conductivity is calculated to be 1.27 W·m⁻¹·K⁻¹. The discrepancy between the thermal conductivity of the 1 mm-thick glass slide and previous high-purity glass (fused silica) is mainly due to the difference in their purity. Van der Tempel et al. [30] have reported the thermal conductivity of borosilicate glass, soda-lime silicate lamp glass, barium strontium silicate glass, and lead silicate glass as 1.45, 1.2, 1.1, and 1.0 W·m⁻¹·K⁻¹ at RT, respectively, showing that glass' thermal conductivity can vary a lot depending on its structure and purities. After this measurement, this 1 mm-thick glass slide is also used in the reference case to measure the thermal conductivity of the two acrylic samples with different thicknesses. Table 2 shows the details of the acrylic samples' experiment. Their thermal conductivity is determined to be 0.20 and 0.19 $W \cdot m^{-1} \cdot K^{-1}$ for the 1.49 mm and 2.81 mm acrylic samples, respectively. Rawas et al. [31] have reported the thermal conductivity of 0.19 and 0.18 W·m⁻¹·K⁻¹ for 2 and 3 mm-thickness acrylic samples, respectively, which agree with our measurement results very well. Moreover, the mechanical engineer's data handbook [32] has reported the acrylic glass' thermal conductivity as 0.2 W·m⁻¹·K⁻¹, which also agrees with our measurement results very well.

To measure the resistance of the black tape and radiationconvection from the black tape surface, we used one-layer black tape as a sample. 3 configurations including 2 layers of black tape, 1 mm-thick glass slide as a reference case, and 1-layer black tape as the sample, we obtain a thermal resistance of 355.6 K·W⁻¹ for combined radiation-convection and 15.6 K W⁻¹ for black tape. The 1-layer black tape's thickness is measured as 0.33 mm, and its thermal conductivity is calculated as 0.329 W·m⁻¹·K⁻¹. Although this resistance (15.6 K-W^{-1}) is the combined black tapes and Al substrate resistances, since Al has low thermal resistance (high thermal conductivity), we consider it approximately equal to the thermal resistance of the black tape. The combined radiation-convection heat transfer coefficient is calculated as 43.9 $W \cdot m^{-2} \cdot K^{-1}$. The estimated contribution of the radiation heat transfer coefficient is calculated as $4\varepsilon\sigma T_0^3 = 4 \times 1 \times 5.67 \times 10^{-8} \times 10^{-8}$ $300^3 = 6.12 \, \mathrm{W} \cdot \mathrm{m}^{-2} \cdot \mathrm{K}^{-1}$. Here ε is the emissivity which takes 1 for the black tape, and σ is the Stefan-Boltzmann constant. Therefore, the estimated contribution of convection heat transfer coefficient is 37.8 W·m⁻²·K⁻¹. The heat transfer coefficient of free convection in the air usually ranges from 2.5-25 W·m⁻²·K⁻¹ [33]. Some tiny forced convection in the air could make this value higher.

3. Out-of-plane thermal conductivity measurement under compressing

In this part, we use the DTR method to measure the very low out-of-plane thermal conductivity of foam at different compression

Table 2 Experimental details of acrylic samples.

	Sample size						
Sample	Length [mm]	Width [mm]	Thickness [mm]	T_1 [°C]	T ₂ [°C]	ΔT [°C]	Q [mW]
Tape (2 layers)	8	8	0.66	23.2	27.6	4.40	240
Glass slide	8	8	1.00	23.0	29.9	6.90	237
Acrylic 1	8	8	1.49	23.3	31.1	7.80	79.3
Acrylic 2	8	8	2.81	23.3	35.1	11.8	79.3

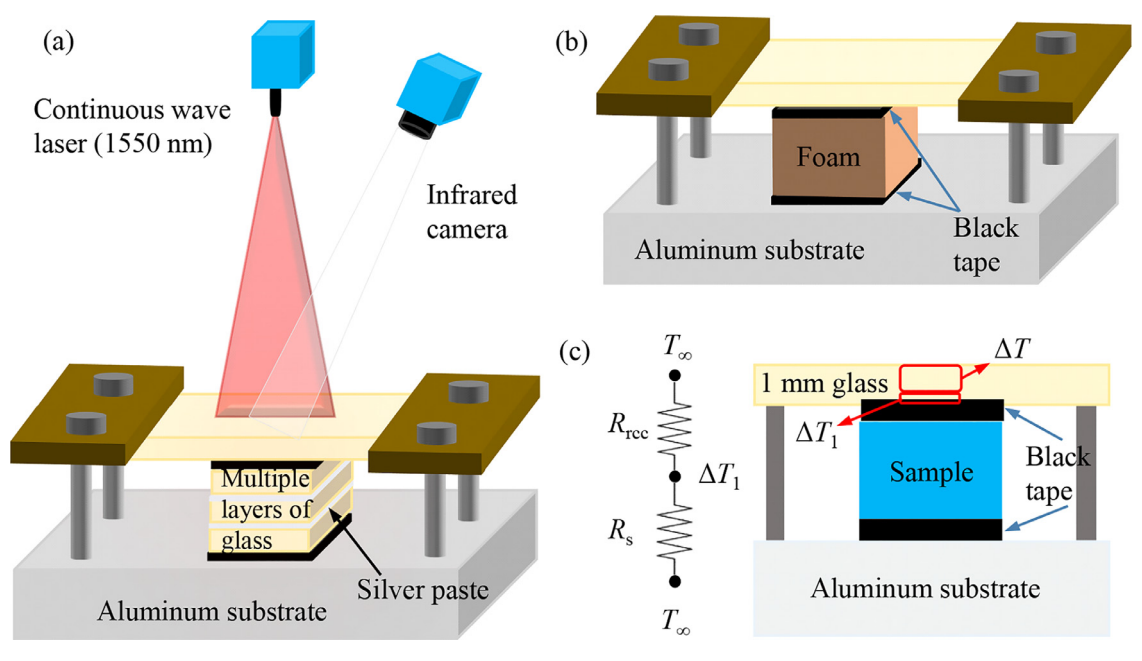


Figure 2. (a) Physical principles, (b) sandwiched sample between Al substrate and glass slide, and (c) thermal resistance circuit of DTR method used to measure the very low thermal conductivity of compressed foam. R_{rcc}: radiation, convection, and conduction (through screws). R_s: sample's thermal resistance. (Not to scale.)

levels. Figure 2(a) shows the physical principles behind this measurement. As Fig. 2(b) shows, the objective sample is sandwiched between the Al substrate and a glass slide (with a thickness of 1 mm), and the two sides of the glass slide are clamped to the Al base using four screws.

Different levels of compression could be achieved by tightening the screws uniformly. The sample is attached to an Al substrate using a double-side black tape, and its top is also coated with a black tape. The above mentioned laser power irradiates the glass surface to penetrate to the sample surface. Since glass is opaque to infrared emission, so the glass surface temperature rise is measured using the above mentioned infrared camera. Figure 2(c) shows the side view of our system with the relevant circuit. Most of the energy of the CW laser is absorbed by the top black tape, and it induces a temperature rise of ΔT_1 at that location. Also, the temperature rise read by the infrared camera is ΔT . This temperature rise is not equal to ΔT_1 due to the effects of the top glass cover on the performance of the camera. These two values are related with a proportionality constant as: $\Delta T = a \times \Delta T_1$. This is due to the steady-state laser heating over the whole heated area. The camera's spectral range is 7.5 to 13 μ m. At room temperature, based on Wien's displacement law [34], the wavelength (λ_{max}) of peak radiation is calculated to be ${\sim}10~\mu m$. The radiation absorption depth (also emission depth) in the glass slide can be calculated as $\tau = \lambda/4\pi k$ [35] to be 0.796 μ m. It is the depth that intensity of the thermal radiation inside the material falls to 1/e of its original value at the surface. k is the extinction coefficient that Kitamura et al. [36] have reported 1 at λ =10 μ m for silica glass slide. This absorption depth is much smaller than glass slide's thickness. Therefore, although the glass slide allows the laser to pass through,

it is effectively opaque for the thermal radiation wavelength. The temperature measured by the infrared camera in fact is its surface temperature. In this configuration, the measured temperature rise is determined by the absorbed laser power, the thermal resistance of radiation-convection, as well as the conduction effects such as conduction through metal screws ($R_{\rm rcc}$) and thermal resistance of the sample ($R_{\rm S}$). Based on this design, the heat transfer equation of this system is written as:

$$\frac{Q}{\Delta T} = a^{-1} \left[\frac{1}{R_{rcc}} + \frac{1}{R_s} \right]. \tag{4}$$

Here, Q is the absorbed laser power. Then, calibration experiments using multiple layers of glass slides with known thermal conductivity are conducted to find a and R_{rcc} . We used 1, 2, and 3-layers of 1 mm thickness glass pieces with a cross-sectional area of 8×8 mm² to obtain the linear relationship between $Q/\Delta T$ and $1/R_s$ to find a and R_{rcc} [shown in Fig. 2(a)]. Note in our measurement, the laser absorption is not perfect. This effect is absorbed in the coefficient a, and will not affect the measurement accuracy. Silver paste is added to their interfaces to ensure a stable and sound thermal connection between the glass layers, and to minimize the effect of interfacial resistance. Note that for each reference experiment, R_s is calculated as: $nL/(k_{glass}A)$. Here n, L, k_{glass} , and A are the number of glass pieces, the thickness of glass layer (1 mm), the thermal conductivity of glass slide (1.27 W·m $^{-1}$ ·K $^{-1}$), and the cross-sectional area of glass pieces (64 \times 10 $^{-6}$ m²), respectively.

Next, a similar experiment is conducted for three foam samples, and the laser heating power and induced temperature rise are recorded. These three foam layers with various compression levels are inserted between the glass cover and substrate. The

Table 3 Experimental details and thermal conductivity of compressed foam samples.

6 1		Sample size			A.T. [0.6]	0 0441
Sample	Compressed by [%]	Length [mm]	Width [mm]	Thickness (after compression) [mm]	ΔT [°C]	Q [W]
Foam 1	0	8	8	1.11	10.0	0.181
Foam 2	50	8	8	1.50	10.7	0.195
Foam 3	75	8	8	1.00	10.2	0.199

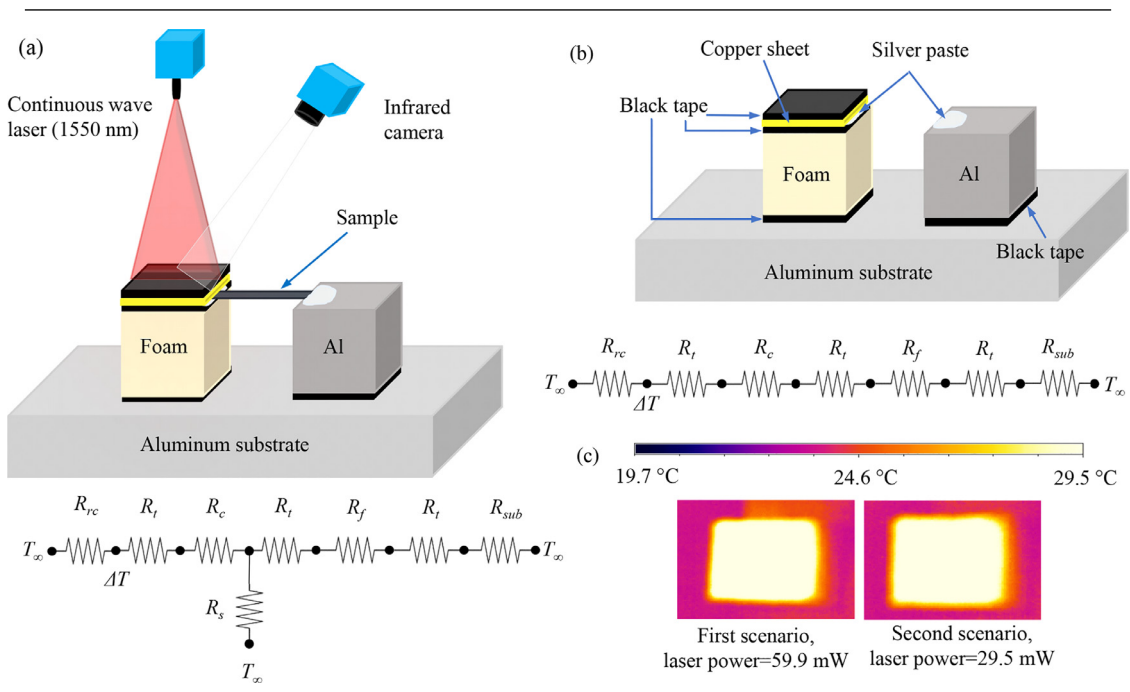


Figure 3. (a) Physical principles of first scenario and its thermal resistance circuit, and (b) second scenario and its thermal resistance circuit of DTR method to measure the in-plane thermal conductivity. R_{rc} : radiation-convection; R_t : black tape; R_c : copper sheet; R_f : foam; R_{sub} : Al substrate; and R_s : sample. (c) Distribution of temperature of two scenarios.

measured values of the out-of-plane foam layers' thermal conductivity are reported in Table 3. Using the measured $Q/\Delta T$ ratio and fitting parameters obtained by the previous experiment, we are able to find the thermal resistance of each foam layer and subsequently their thermal conductivity as: $k_f = L/(R_{foam}A)$. The foam's thermal conductivity in the air is determined to be 0.064, 0.102, and 0.174 $W \cdot m^{-1} \cdot K^{-1}$ for compression levels of 0%, 50%, and 75%, respectively. It is shown that the thermal conductivity of the foam is increased by the increased compression level. This is justified by the reduced porous structure of the compressed foam. For first order estimation, the foam's thermal conductivity can be expressed as $k_f = \varphi k_{blk}/3$. Here, φ is the volume fraction of the solid phase in the foam, and k_{blk} is the intrinsic thermal conductivity of the solid part in the foam [37]. The ratio k of 50% and 75% compression over the k without compression is 1.55 and 2.72, which is lower than the first order estimation ratio (2 and 4). This showed increase of k with compression can be explained by the nonlinear effect which has been expressed by the Maxwellian equation: $k_f/k_{blk} = \alpha^{-1} + 3(\alpha - 1)\varphi/[\alpha(\alpha + 2 - (\alpha - 1)\varphi)]$, where $\alpha = k_{blk}/k_{air}$ [38]. Take an instance for $\alpha = 5$, k_f/k_{blk} will be 0.236, 0.277, and 0.378 for $\varphi = 0.1$, 0.2, and 0.4, demonstrating the nonlinear thermal conductivity increase with the compression level.

4. DTR measurement of in-plane thermal conductivity at the microscale

4.1. Experimental principles

In this part, we introduce the DTR method for the in-plane thermal conductivity measurement at the microscale, Figure 3(a)

shows the physical principles of the first scenario of this measurement. In this scenario, the sample is suspended between the foam and an Al block. The foam is attached to an Al substrate using a double-side black tape, and its top is also coated with a black tape. On top of it, the sample is attached under a thin copper foil (0.096 mm) with silver paste. Using silver paste and copper foil, which have high thermal conductivity, ensures good thermal contact, heat transfer, and uniform surface temperature. The top of the copper foil is also covered with black tape to ensure well-defined laser energy absorption with negligible reflection. The other part of the suspended sample is attached to a large Al block with silver paste. Using the large Al block and silver paste with good thermal conductivity ensures that heat is transferred away from the sample instead of accumulating there. As a result, it does not affect the temperature rise of the sample. Also, using foam under the sample ensures that most of the heat is transferred from sample to the Al block and increases the accuracy and sensitivity of the measurement.

The above mentioned laser irradiates the top tape surface, and the surface temperature rise is measured using the above mentioned infrared camera. In this configuration, the measured temperature rise is determined by the absorbed laser power, the thermal resistance of the sample (R_s) , the thermal resistance of the three black tapes (R_t) , thermal resistance of the radiation-convection (R_{rc}) on the tape surface, thermal resistance of the copper sheet (R_c) , thermal resistance of the foam (R_f) , and the thermal resistance of the substrate (R_{sub}) . The relevant circuit is shown in Fig. 3(a). Figure 3(b) shows the physical principles of the second scenario. In this scenario, the sample is removed entirely, but the other parts of the experiment remain as same as in the first

scenario. The temperature rise caused by laser irradiation is measured using the infrared camera again. In this configuration, the measured temperature rise is determined by the absorbed laser power, R_c , R_f , and R_{sub} . The relevant circuit is shown in Fig. 3(b). The laser spot is large enough to cover the entire tape surface, and the irradiated laser energy is measured using a power meter with sound accuracy in both scenarios. Figure 3(c) shows the uniform temperature distribution of this experiment's first and second scenarios. It is obvious the sample's surface has a very uniform temperature, with a nonuniformity better than 0.5 °C. Details of uncertainty analysis are provided later.

The thermal conductivity of the sample is obtained using this equation $k_s = t_s/(R_s A_s)$. Here, t_s is the sample thickness which is measured by a digital micrometer, and A_s is the side area of the sample. For all the two thermal circuits in Fig. 3(a) and (b), the governing equations are:

$$Q_1 = \Delta T_1 \left[\frac{1}{R_{rc}} + \frac{1}{R_{tc} + \left[R_{tot}^{-1} + R_s^{-1} \right]^{-1}} \right], \tag{5}$$

$$Q_2 = \Delta T_2 \left[\frac{1}{R_{rc}} + \frac{1}{R_{tc} + R_{tot}} \right]. \tag{6}$$

Here, subscript "tc" represents combinations of upper black tape and copper sheet, and subscript "tot" represents the combination of middle and lower black tapes, foam, and Al substrate. Q_1 , Q_2 , ΔT_1 , and ΔT_2 are laser powers and temperature rise related to the first and second scenarios, respectively. We used radiation-convection and tape resistance measured earlier for R_{rc} and R_{tc} , respectively. Here R_{tc} is the combined upper black tape and copper sheet resistances. Since copper sheet has a negligible thermal resistance (very high thermal conductivity) compared with that of the black tape, we consider it negligible. R_{tot} will be determined by solving Eq. (6). Then by replacing R_{tot} into Eq. (5), the sample's thermal resistance can be obtained.

4.2. Measurement of reference material

In this part, the thermal conductivity of graphene paper (highly conductive graphene from Graphene Supermarket) is measured using the DTR method to access the measurement accuracy. Table 4 shows the details of the graphene paper experiment. In this table, T_1 and T_2 represent the top tape surface temperature before and after laser irradiation, respectively. ΔT shows the temperature rise caused by laser irradiation. For three different sizes of graphene papers, the thermal conductivity is measured to be 616, 631, and 642 W·m⁻¹·K⁻¹. Xie et al. [39] reported the thermal conductivity of the same graphene paper at room temperature (RT) to be in the range of 634-710 W·m⁻¹·K⁻¹, which agrees well with our measurement results.

4.3. Measurement of micron-thick copper foil

In this part, first, the in-plane thermal conductivity of micronthick copper foil (copper foil roll from Uxcell) is measured using the DTR method, then its electrical conductivity is measured with the four-probe technique, and its Lorenz number is determined to access the measurement accuracy. Table 5 shows the details of copper foil's thermal conductivity experiment. In this table, T_1 and T_2 represent the top tape surface temperature before and after laser irradiation, respectively. ΔT is the temperature rise caused by laser irradiation. The thermal conductivity of the copper foil is measured to be 322 W·m⁻¹·K⁻¹. The small discrepancy between our results and those of mechanical engineer's data handbook [32], which is 386 W·m⁻¹·K⁻¹, can be explained by the density of the copper foil used in this experiment, which is measured

Table 4 Experimental details of graphene paper

		1 1 0									
:	Sample size			T ₁ [°C]		T ₂ [°C]		ΔT [°C]		Q [mW]	
Ö.	. Width [mm]	Thickness [mm]	Length [mm]	First scenario	Second scenario	First scenario	Second scenario	First scenario	Second scenario	First scenario	Second scenario
-	2.67	0.026	4.34	23.4	23.4	28.1	40.0	4.70	16.6	54.4	51.6
7	2.36	0.027	4.57	23.2	23.2	28.0	40.0	4.80	16.8	51.6	51.6
3	2.13	0.026	4.83	23.3	23.3	28.2	37.3	4.90	14.0	48.8	48.8

Table 5 Experimental details of cooper foil.

No.	Sample size			T_1 [°C]		T ₂ [°C]		Δ <i>T</i> [°C]		Q [mW]	
	Width [mm]	Thickness [mm]	Length [mm]	First scenario	Second scenario	First scenario	io Second scenario	First scenario	Second scenario	First scenario	irst scenario Second scenario
1	2.56	0.015	4.68	23.3	23.3	28.4	31.7	5.10	8.40	29.5	26.6

to be 7.96 g·cm $^{-3}$ at RT. While mechanical engineer's data handbook [32] has reported the pure copper density of 8.93 g·cm $^{-3}$, proving that our copper foil is not full dense. Based on the density, the air/pore volume fraction in the copper coil is calculated to be 0.1086. Based on the Maxwellian equation [38], the copper foil's thermal conductivity is calculated to be 326 W·m $^{-1}$ ·K $^{-1}$, which is very close to our measurement result of 322 W·m $^{-1}$ ·K $^{-1}$.

In addition to thermal conductivity, the four-probe technique is used to measure the electrical conductivity of the micron-thick copper foil to have a further understanding of this material. In the four-probe technique, as Fig. 4(a) shows, a DC current (Keithley 6221) is applied between the two outer probes (1 and 4), and the induced voltage between two inner probes (2 and 3) is measured by a very high-precision multimeter (Keithley 2002, 8.5 digits). Figure 4(b) shows the experimental setup of the four-probe technique in our lab. Probes are located on a 3D micro-stage to easily establish the contact between tips and copper foil.

The following equation is used to calculate the electrical conductivity of the micron-thick copper foil:

$$\sigma^{-1} = F_1 F_2 F_3 t V / I. \tag{7}$$

Here *t* is copper foil thickness, *V* is the voltage drop over probe 2 and 3, and I is the current. F_1 is the finite shape correction factor that can be derived from the standard table [40]. F_2 is the probe tip spacing correction factor and can be calculated from this equa $tionF_2 = 1 + 1.082[1 - S_2/s]$. Here, S_2 is the space between the two inner probes (2 and 3), and s is the average probe tip spacing. In this experiment, since probe tips are equally spaced, F_2 equals to one. F_3 is the thickness correction factor that takes 1 in this experiment since the $t/s \ll 0.4$ [40]. Note that, in this experiment, the average probe spacing s is 1.667 mm while the foil thickness is only 0.015 mm. We obtained the electrical conductivity of copper foil in the range of (4.73-4.91) \times 10⁷ Ω^{-1} m⁻¹, as shown in Table 6, while Raab et al. [41] have reported it for the 99.9% pure copper as 5.58 \times $10^7~\Omega^{-1}~m^{-1},$ again proving that our copper foil is not full dense, since electrical conductivity decreases with decreased density. Based on the Maxwellian equation [38], the copper foil's electrical conductivity is calculated to be 4.72 \times 10⁷ Ω^{-1} ·m⁻¹ which is very close to our measurement result of $(4.73-4.91) \times 10^7$ $\Omega^{-1} \cdot m^{-1}$.

The Lorenz number can be obtained as $k/\sigma = LT$. Here L is the Lorenz number, T is the RT which is 296 K, k is the thermal conductivity measured by the DTR method, and σ is the electrical conductivity measured by the four-probe technique. Table 6 shows the experimental details of the measurement, electrical conductivity, and Lorenz number of the copper foil. Note that, in this experiment, the copper foil sample is a square piece with side d. As table 6 shows, we obtained the Lorenz number at RT in the range of $(2.21\text{-}2.30) \times 10^{-8} \text{ W}\cdot\Omega\cdot\text{K}^{-2}$. Reference data [42] reported on the Lorenz number for pure copper is in the range of $(2.23\text{-}2.33) \times 10^{-8} \text{ W}\cdot\Omega\cdot\text{K}^{-2}$ at 0 °C to 100 °C, which is very close to our measurement results.

5. Discussions and uncertainty

The focus of this study is developing a new technique to overcome the challenges of other techniques, not the study of different materials' thermal conductivity. Although we have measured the thermal conductivity of some limited materials, this technique can be also used for polymer-based composites. In this part, the uncertainty of the thermal conductivity measurement due to the effect of radiation-convection around the sample is calculated and analyzed. For measuring thermal conductivity, the effect of radiation-convection can be calculated by: $\Delta k_{rad+conv} = PhL^2/(\pi^2 A)$ [43,44]. Here, P is the perpendicular surface perimeter to the direction of heat transfer direction, h is the combined radiation-convection

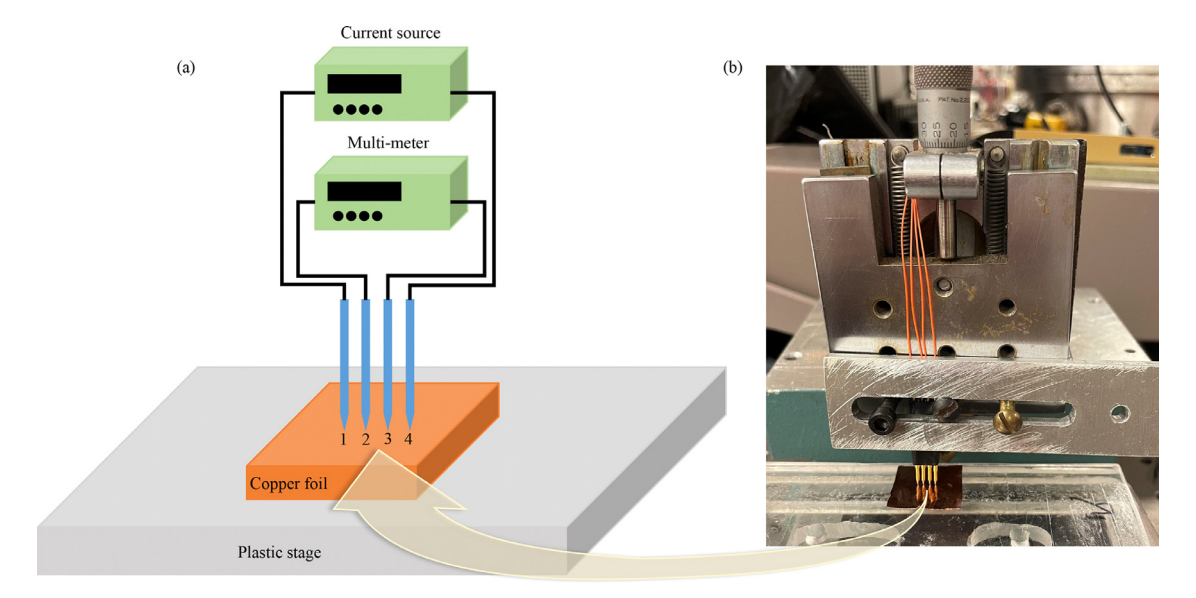


Figure 4. (a) Schematic and (b) experimental setup of the four-probe technique.

Table 6Experimental details, electrical conductivity, and Lorenz number of the micron-thick copper foil.

No.	I [mA]	<i>V</i> [mV]	d [mm]	t [mm]	F ₁	$\sigma~[10^7~\Omega^{-1}{\cdot}m^{-1}]$	L [10 ⁻⁸ W·Ω·K ⁻²]
1 2	100 100	0.0370 0.0329	10 20	0.015 0.015	3.7096 4.2878	4.86 4.73	2.24 2.30
3	100	0.0304	40	0.015	4.4636	4.91	2.21

Table 7Uncertainty of out-of-plane thermal conductivity caused by radiation and convection.

Sample	Thickness [mm]	$\Delta k_{rad+conv}/k$ [%]
1-mm glass slide	1.00	0.157
Acrylic 1	1.49	2.50
Acrylic 2	2.81	8.94

Table 8Uncertainty of in-plane thermal conductivity caused by radiation and convection.

Length[mm]	$\Delta k_{rad+conv}/k$ [%]
4.34	1.05
4.57	1.10
4.83	1.13
	4.34 4.57

heat transfer coefficient measured earlier as 43.9 W·m⁻²·K⁻¹, *L* is the length in the heat conduction direction, and *A* is the heat conduction cross-sectional area. Tables 7 and 8 show the uncertainty of our out-of-plane and in-plane thermal conductivity measurements caused by radiation and convection, respectively. The 1 mm glass slide is the thinnest one, and the acrylic sample 2 is the thickest one for out-of-plane thermal conductivity measurement. As expected, the radiation-convection uncertainty increases with increased sample thickness, as shown in Table 7. A thicker sample increases the side sample surface, resulting in a stronger radiation-convection effect. For in-plane thermal conductivity, the same explanation applies as for sample length. However, the measurements can be conducted in a vacuum chamber to eliminate the convection effects.

In our thermal conductivity measurement, there was another uncertainty caused by sample size, temperature rise, and laser power measurement. In the out-of-plane thermal conductivity experiment, the measurement uncertainty of the thickness, area,

temperature rise, and laser power were 3.3×10^{-3} %, 8.8%, 0.064%, and 0.17%, respectively. Therefore, the uncertainty of the thermal conductivity measurement was 8.8%. In the in-plane thermal conductivity experiment, the measurement uncertainty of the length, area, temperature rise, and laser power were 1.1×10^{-3} %, 0.19%, 0.11%, and 0.25%, respectively. Therefore, the uncertainty of thermal conductivity measurement was 0.33%. Note that in this technique, samples were heated by laser irradiation on their surface. Therefore, no electrical conductive properties of samples were used, and it did not influence the measurements' uncertainty.

To test the experiment's reproducibility due to the black tape attachment condition, we used one acrylic sample and changed the attached tapes five times on both sides. Table 9 shows the details of the experiment. The thermal conductivity of acrylic is measured to be $0.206\pm0.005~\rm W\cdot m^{-1}\cdot K^{-1}$, which proves the experiment's excellent reproducibility under the black tape attachment condition. To test the experiment's reproducibility, we measured the thermal conductivity of 4 different acrylic samples. Table 10 shows the details of the experiment. The thermal conductivity of acrylic is measured to be $0.205\pm0.006~\rm W\cdot m^{-1}\cdot K^{-1}$, which proves that the experiment has sound reproducibility.

For the DTR methodology presented in this work, it can be extended generally as below. For a certain configuration, different reference samples of similar thickness/geometries like that of the sample can be measured to establish the surface temperature rise $\Delta T \sim R$ correlation (R: reference sample's thermal resistance) under the same level laser heating condition. The sample of interest can be used to make one configuration and measure the temperature rise as ΔT_s . This temperature rise then is used in the calibrated $\Delta T \sim R$ correlation to extract the sample's thermal resistance, and finally determine its thermal conductivity. For this methodology, in fact the exact laser absorption value is not needed as long as the temperature rise is measured and normalized to the same laser heating condition. This provides great advantages in measurement control and ensures very high measurement accuracy.

 Table 9

 Experimental detail of acrylic sample for testing reproducibility due to the black tape attachment condition.

	Sample Size					AT [0C]	
Sample	Length [mm]	Width [mm]	Thickness [mm]	T_1 [°C]	T ₂ [°C]	ΔT [°C]	Q [mW]
Tape (2 layers)	8.00	8.00	0.66	23.2	27.6	4.40	240
Glass slide	8.00	8.00	1.00	23.0	29.9	6.90	237
Acrylic	7.97	7.97	1.54	23.2	31.4	8.20	79.3
Acrylic	7.97	7.97	1.54	23.4	30.9	7.50	76.6
Acrylic	7.97	7.97	1.54	23.4	31.1	7.70	79.3
Acrylic	7.97	7.97	1.54	23.5	31.7	8.20	82.1
Acrylic	7.97	7.97	1.54	23.5	31.2	7.70	79.3

Table 10 Experimental details of 4 acrylic samples for testing experiment's reproducibility.

	Sample Size						
Sample	Length [mm]	Width [mm]	Thickness [mm]	T_1 [°C]	<i>T</i> ₂ [°C]	ΔT [°C]	Q [mW]
Tape (2 layers)	8.00	8.00	0.66	23.2	27.6	4.40	240
Glass slide	8.00	8.00	1.00	23.0	29.9	6.90	237
Acrylic 1	8.09	7.94	1.53	23.5	30.8	7.30	73.8
Acrylic 2	8.03	7.98	1.53	23.3	30.9	7.60	76.6
Acrylic 3	7.97	7.97	1.54	23.2	31.4	8.20	79.3
Acrylic 4	8.00	8.00	1.49	23.3	31.1	7.80	79.3

6. Conclusion

In this paper, a differential methodology was successfully developed to characterize the out-of-plane thermal conductivity of the few mm-thick samples, extremely low out-of-plane thermal conductivity of foam at different compression levels, and the inplane thermal conductivity of micro-thick samples. Employing this new method, we measured acrylic glass, glass slide, graphene paper, and copper foil. The measurement results agree well with either reference values or measurement using other techniques. Also, we calculated the Lorenz number of the copper foil based on its electrical conductivity measured using the four-probe technique. The measurement results (2.21-2.30) \times 10⁻⁸ W· Ω ·K⁻² agreed well with the reference values of (2.23-2.33) \times 10⁻⁸ W· Ω ·K⁻². Our uncertainty analysis showed that the radiation-convection effects and sample size, temperature rise, and laser power measurements all caused small measurement uncertainty, usually around $1\sim2\%$. Moreover, the convection effect can be eliminated by conducting the experiment in vacuum, which will bring the measurement accuracy to a higher level. The DTR methodology can be generalized by measuring different reference samples of similar thickness like that of the sample to establish the surface temperature rise $\Delta T \sim R$ correlation (R: reference sample's thermal resistance) under the same level laser heating condition. The temperature rise ΔT_s of sample of interest can be used to extract its thermal resistance and thermal conductivity from the calibrated $\Delta T \sim R$ correlation. The DTR technology in fact does not need the exact laser absorption value and provides great advantages in measurement control and ensures very high measurement accuracy.

Declaration of Competing Interest

The authors declare that they have no known competing financial interests or personal relationships that could have appeared to influence the work reported in this paper.

CRediT authorship contribution statement

Mahya Rahbar: Data curation, Investigation, Formal analysis, Writing – review & editing. **Meng Han:** Data curation, Investigation, Formal analysis, Writing – review & editing. **Shen Xu:** Methodology, Validation, Writing – review & editing. **Hamidreza**

Zobeiri: Data curation, Investigation, Formal analysis, Methodology, Validation, Writing – review & editing. **Xinwei Wang:** Conceptualization, Conceptualization, Funding acquisition, Writing – review & editing.

Data availability

Data will be made available on request.

Acknowledgment

Partial support of this work by US National Science Foundation (CBET1930866 and CMMI2032464 for X. W.) is gratefully acknowledged.

References

- [1] S.G. Mosanenzadeh, H.E. Naguib, Effect of filler arrangement and networking of hexagonal boron nitride on the conductivity of new thermal management polymeric composites, Compos. Part B Eng. 85 (2016) 24–30.
- [2] H. Fekiri, V.A. Esin, V. Maurel, A. Köster, Y. Bienvenu, Microstructure evolution of innovative thermal bridge composite (i-TBC) for power electronics during elaboration, Mater. Des. 137 (2018) 68–78.
- [3] B. Tian, W. Yang, L. Luo, J. Wang, K. Zhang, J. Fan, J. Wu, T. Xing, Synergistic enhancement of thermal conductivity for expanded graphite and carbon fiber in paraffin/EVA form-stable phase change materials, Solar Energy 127 (2016) 48–55.
- [4] G. Yuan, X. Li, Z. Dong, X. Xiong, B. Rand, Z. Cui, Y. Cong, J. Zhang, Y. Li, Z. Zhang, Pitch-based ribbon-shaped carbon-fiber-reinforced one-dimensional carbon/carbon composites with ultrahigh thermal conductivity, Carbon 68 (2014) 413–425.
- [5] I. Mazov, I. Burmistrov, I. Il'inykh, A. Stepashkin, D. Kuznetsov, J.P. Issi, Anisotropic thermal conductivity of polypropylene composites filled with carbon fibers and multiwall carbon nanotubes, Polym. Compos. 36 (11) (2015) 1951–1957.
- [6] W. Parker, R. Jenkins, C. Butler, G. Abbott, Flash method of determining thermal diffusivity, heat capacity, and thermal conductivity, J. Appl. Phys. 32 (9) (1961) 1679–1684.
- [7] M. Boutinguiza, F. Lusquiños, J. Pou, R. Soto, F. Quintero, R. Comesaña, Thermal properties measurement of slate using laser flash method, Opt. Lasers Eng. 50 (5) (2012) 727–730.
- 8] B.B. Czél, K.A. Woodbury, J. Woolley, G. Gróf, Analysis of parameter estimation possibilities of the thermal contact resistance using the laser flash method with two-layer specimens, Int. J. Thermophys. 34 (10) (2013) 1993–2008.
- [9] J. Guo, X. Wang, T. Wang, Thermal characterization of microscale conductive and nonconductive wires using transient electrothermal technique, J. Appl. Phys. 101 (6) (2007) 063537.
- [10] B. Feng, W. Ma, Z. Li, X. Zhang, Simultaneous measurements of the specific heat and thermal conductivity of suspended thin samples by transient electrothermal method, Rev. Sci. Instrum. 80 (6) (2009) 064901.

- [11] C. Xing, T. Munro, C. Jensen, H. Ban, Analysis of the electrothermal technique for thermal property characterization of thin fibers, Meas. Sci. Technol. 24 (10) (2013) 105603.
- [12] T. Wang, X. Wang, J. Guo, Z. Luo, K. Cen, Characterization of thermal diffusivity of micro/nanoscale wires by transient photo-electro-thermal technique, Appl. Phys. A 87 (4) (2007) 599–605.
- [13] J. Liu, M. Han, R. Wang, S. Xu, X. Wang, Photothermal phenomenon: extended ideas for thermophysical properties characterization, J. Appl. Phys. 131 (6) (2022) 065107.
- [14] L. Lu, W. Yi, D. Zhang, 3ω method for specific heat and thermal conductivity measurements, Rev. Sci. Instrum. 72 (7) (2001) 2996–3003.
- [15] W. Yi, L. Lu, Z. Dian-Lin, Z. Pan, S. Xie, Linear specific heat of carbon nanotubes, Phys. Rev. B 59 (14) (1999) R9015.
- [16] C. Xing, T. Munro, C. Jensen, H. Ban, C.G. Copeland, R.V. Lewis, Thermal characterization of natural and synthetic spider silks by both the 3ω and transient electrothermal methods, Mater. Des. 119 (2017) 22–29.
- [17] J. Hou, X. Wang, J. Guo, Thermal characterization of micro/nanoscale conductive and non-conductive wires based on optical heating and electrical thermal sensing, J. Phys. D Appl. Phys. 39 (15) (2006) 3362–3370.
- [18] J. Hou, X. Wang, C. Liu, H. Cheng, Development of photothermal-resistance technique and its application to thermal diffusivity measurement of single-wall carbon nanotube bundles, Appl. Phys. Lett. 88 (18) (2006) 181910.
- [19] J. Hou, X. Wang, L. Zhang, Thermal characterization of submicron polyacrylonitrile fibers based on optical heating and electrical thermal sensing, Appl. Phys. Lett. 89 (15) (2006) 152504.
- [20] J. Guo, X. Wang, D. Geohegan, G. Eres, C. Vincent, Thermal characterization of micro/nanoscale wires/tubes using pulsed laser-assisted thermal relaxation, in: MRS Online Proceedings Library (OPL), Vol. 1083, 2008.
- [21] J. Guo, X. Wang, D.B. Geohegan, G. Eres, Thermal characterization of multi-wall carbon nanotube bundles based on pulsed laser-assisted thermal relaxation, Funct. Mater. Lett. 1 (1) (2008) 71–76.
- [22] J. Guo, X. Wang, D.B. Geohegan, G. Eres, C. Vincent, Development of pulsed laser-assisted thermal relaxation technique for thermal characterization of microscale wires, J. Appl. Phys. 103 (110) (2008) 113505.
- [23] S. Sandell, E. Chávez-Ángel, A. El Sachat, J. He, C.M. Sotomayor Torres, J. Maire, Thermoreflectance techniques and Raman thermometry for thermal property characterization of nanostructures, J. Appl. Phys. 128 (13) (2020) 131101.
- [24] J. Zhu, X. Wu, D.M. Lattery, W. Zheng, X. Wang, The ultrafast laser pump-probe technique for thermal characterization of materials with micro/nanostructures, Nanoscale Microscale Thermophys. Eng. 21 (3) (2017) 177–198.
- [25] P. Jiang, X. Qian, R. Yang, Tutorial: time-domain thermoreflectance (TDTR) for thermal property characterization of bulk and thin film materials, J. Appl. Phys. 124 (16) (2018) 161103.
- [26] A.J. Schmidt, R. Cheaito, M. Chiesa, A frequency-domain thermoreflectance method for the characterization of thermal properties, Rev. Sci. Instrum. 80 (9) (2009) 094901.

- [27] A.J. Schmidt, R. Cheaito, M. Chiesa, Characterization of thin metal films via frequency-domain thermoreflectance, J. Appl. Phys. 107 (2) (2010) 024908.
- [28] J. Zhu, D. Tang, W. Wang, J. Liu, K.W. Holub, R. Yang, Ultrafast thermore-flectance techniques for measuring thermal conductivity and interface thermal conductance of thin films, J. Appl. Phys. 108 (9) (2010) 094315.
- [29] T.L. Bergman, T.L. Bergman, F.P. Incropera, D.P. Dewitt, A.S. Lavine, in: Fundamentals of Heat and Mass Transfer, seventh ed., John Wiley & Sons, 2011, p. 993.
- [30] L. van der Tempel, G.P. Melis, T. Brandsma, Thermal conductivity of a glass: I. Measurement by the glass-metal contact, Glass Phys. Chem. 26 (6) (2000) 606–611.
- [31] A.S.A. Rawas, M.Y. Slewa, E.G. Yonis, Improvement of thermal conductivity and mechanical properties of cold curing acrylic material, Int. J. Enhanced Res. Sci. Eng. 4 (4) (2015) 187–192.
- [32] J. Čarvill, in: Thermodynamics and Heat Transfer, Mechanical Engineer's Data Handbook, J. Carvill Butterworth-Heinemann, 1993, pp. 102–145.
- [33] P. Kosky, R. Balmer, W. Keat, G. Wise, in: Exploring Engineering, fifth ed., Academic Press, 2021, pp. 317–340.
- [34] B. Das, Obtaining Wien's displacement law from Planck's law of radiation, Phys. Teacher 40 (3) (2002) 148–149.
- [35] M.A. Green, M.J. Keevers, Optical properties of intrinsic silicon at 300 K, Prog. Photovolt. Res. Appl. 3 (3) (1995) 189–192.
- [36] R. Kitamura, L. Pilon, M. Jonasz, Optical constants of silica glass from extreme ultraviolet to far infrared at near room temperature, Appl. Opt. 46 (33) (2007) 8118–8133.
- [37] L. Huan, X. Shen, W. Xinwei, M. Ning, Significantly reduced thermal diffusivity of free-standing two-layer graphene in graphene foam, Nanotechnology 24 (41) (2013) 415706 2013.
- [38] X. Wang, X. Xu, S.U.S. Choi, Thermal conductivity of nanoparticle fluid mixture, J. Thermophys. Heat Transf. 13 (4) (1999) 474–480.
- [39] Y. Xie, P. Yuan, T. Wang, N. Hashemi, X. Wang, Switch on the high thermal conductivity of graphene paper, Nanoscale 8 (40) (2016) 17581–17597.
- [40] F. Smits, Measurement of sheet resistivities with the four-point probe, Bell Syst. Tech. J. 37 (3) (1958) 711–718.
- [41] S. Raab, R. Guschlbauer, M. Lodes, C. Körner, Thermal and electrical conductivity of 99.9% pure copper processed via selective electron beam melting, Adv. Eng. Mater. 18 (9) (2016) 1661–1666.
- [42] C. Kittel, P. McEuen, in: Kittel's Introduction to Solid State Physics, eighth ed., John Wiley & Sons, 2018, pp. 156–157.
- [43] Y. Xie, H. Zobeiri, L. Xiang, G. Eres, J. Wang, X. Wang, Dual-pace transient heat conduction in vertically aligned carbon nanotube arrays induced by structure separation, Nano Energy 90 (2001) 106516.
- [44] H. Lin, S. Xu, X. Wang, N. Mei, Significantly reduced thermal diffusivity of free-standing two-layer graphene in graphene foam, Nanotechnology 24 (41) (2013) 415706.